Moment inference from tomograms

F. D. Day-Lewis,[1] Y. Chen,[2] and K. Singha[3]

Received 17 August 2007; revised 10 October 2007; accepted 22 October 2007; published 22 November 2007.

[1] Time-lapse geophysical tomography can provide valuable qualitative insights into hydrologic transport phenomena associated with aquifer dynamics, tracer experiments, and engineered remediation. Increasingly, tomograms are used to infer the spatial and/or temporal moments of solute plumes; these moments provide quantitative information about transport processes (e.g., advection, dispersion, and rate-limited mass transfer) and controlling parameters (e.g., permeability, dispersivity, and rate coefficients). The reliability of moments calculated from tomograms is, however, poorly understood because classic approaches to image appraisal (e.g., the model resolution matrix) are not directly applicable to moment inference. Here, we present a semi-analytical approach to construct a moment resolution matrix based on (1) the classic model resolution matrix and (2) image reconstruction from orthogonal moments. Numerical results for radar and electrical-resistivity imaging of solute plumes demonstrate that moment values calculated from tomograms depend strongly on plume location within the tomogram, survey geometry, regularization criteria, and measurement error. **Citation:** Day-Lewis, F. D., Y. Chen, and K. Singha (2007), Moment inference from tomograms, *Geophys. Res. Lett.*, *34*, L22404, doi:10.1029/2007GL031621.

1. Introduction

[2] Geophysical tomography has been used to monitor mass transport associated with tracer experiments [e.g., *Day-Lewis et al.*, 2003; *Singha and Gorelick*, 2005, 2006], infiltration tests [e.g., *Binley et al.*, 2002], engineered remediation [e.g., *Lane et al.*, 2004, 2006], and other transport processes. Tomograms serve as time-lapse snapshots of geophysical properties (e.g., electrical resistivity or radar attenuation) that can be related to hydrologic parameters of interest (e.g., tracer concentration); hence they provide valuable information for construction and calibration of numerical models of flow and transport. In several studies [*Hubbard et al.*, 2001; *Singha and Gorelick*, 2005; *Binley et al.*, 2002], plume moments were inferred from time-lapse tomograms. Moment inference provides direct insight into transport processes and controlling parameters. The reliability of moment inference from tomograms, however, remains poorly understood.

[3] In using moments calculated from tomograms, it is assumed that the tomogram provides an adequate approximation of the solute plume; the resolution of tomographic estimates, however, is known to be a function of survey geometry, measurement physics, measurement error, regularization, and parameterization [e.g., *Day-Lewis and Lane*, 2004; *Day-Lewis et al.*, 2005]. The model resolution matrix, **R**, is commonly used to quantify tomographic resolving power:

$$\mathbf{R} = \left[\mathbf{J}^T\mathbf{W}^T\mathbf{W}\mathbf{J} + \beta\mathbf{D}^T\mathbf{D}\right]^{-1}\mathbf{J}^T\mathbf{W}^T\mathbf{W}\mathbf{J} \quad (1)$$

where

- **J** Jacobian of predicted measurements with respect to model parameters, m;
- **W** diagonal matrix where W_{ii} is the reciprocal of the standard error for measurement i;
- **D** Tikhonov regularization matrix (e.g., second-derivative filter); and
- β tradeoff parameter between the regularization and measurement fitting.

[4] The model resolution matrix is a powerful tool for understanding how well a given survey will resolve a hypothetical target. For linear problems, $\hat{\mathbf{m}} = \mathbf{R}\mathbf{m}$, where $\hat{\mathbf{m}}$ is the vector of tomographic model estimates and **m** is the vector of true model parameters; for nonlinear problems, **R** is commonly calculated for the final iteration of the inversion, and $\hat{\mathbf{m}} \approx \mathbf{R}\mathbf{m}$, where the approximation degrades with increasing nonlinearity. For the case of perfect resolution, **R** is an identity matrix and parameter estimates are independent. More commonly, resolution is imperfect, the geophysical parameter estimates represent local averages, and tomograms are smooth, blunted versions of reality. In such cases, moments calculated on tomograms may be unreliable. The objective of this research is to quantify how well the moments calculated from tomograms reflect the moments of the true image, and how the quality of inferred moments depends on regularization criteria, measurement error, and survey geometry. Toward this end, we derive a formulation for a new resolution matrix for moment inference from tomograms.

2. Inferring Plume Moments From Tomograms

[5] The spatial and temporal distributions of solute plumes are commonly characterized by geometric moments [e.g., *Singha and Gorelick*, 2005]. Geometric moments provide direct insight into the effects of advection, dispersion, and other processes controlling the migration of solute plumes. The zero-order moment describes the total mass; the first-order moments are related to the center of mass; the second-order moments describe the spread and are related to dispersion; and higher order moments are used to describe

[1] U.S. Geological Survey, Office of Ground Water, Branch of Geophysics, Storrs, Connecticut, USA.
[2] Center for Integrative Geosciences, University of Connecticut, Storrs, Connecticut, USA.
[3] Department of Geosciences, Pennsylvania State University, University Park, Pennsylvania, USA.

0094-8276/07/2007GL031621

non-Gaussian plumes that have undergone degradation reactions, slow advection, and/or rate-limited mass transfer [e.g., *Harvey and Gorelick*, 1995]. For a pixilated two-dimensional image, geometric moments are given by

$$\mu_{p,q} = \sum_{i=1}^{nx \cdot nz} m_i x_i^p z_i^q \Delta x \Delta z \tag{2}$$

where

- $\mu_{p,q}$ geometric moment of order p in the x direction, and q in the z direction, with overall order $N = p + q$; for example, $\mu_{0,2}$ is the zero-order moment in x and second-order moment in z.
- m_i parameter of interest in pixel i;
- x_i, z_i coordinates at the center of pixel i in the x and z directions, respectively, and x,z $\in$([−X,X],[−Z,Z]);
- Δx, Δz pixel dimensions in the x and z directions, respectively;
- nx, nz number of pixels in the x and z directions; and
- i pixel index, which cycles fastest on x; i.e., $i = (iz - 1)nx + ix$.

[6] To facilitate the derivations and presentation that follow, we recast equation (2) as a matrix operation, $\boldsymbol{\mu} = \mathbf{Gm}$, where the components of $\mathbf{G}$ are the products of the powers of x and z for corresponding pixels and moment orders, and the moment values in $\boldsymbol{\mu}$ are arranged such that the vector elements cycle first on the moment order and secondly on direction, with x first:

$$\boldsymbol{\mu} = \left[\mu_{0,0}\mu_{0,1}\mu_{1,0}\mu_{0,2}\mu_{1,1}\mu_{2,0}\ldots\mu_{N,0}\right] \tag{3}$$

The zero- through second-order moments are related to the center of mass and spread by:

$$\mu_{\mathrm{xc}} = \mu_{1,0}/\mu_{0,0}, \tag{4a}$$

$$\mu_{\mathrm{zc}} = \mu_{1,0}/\mu_{0,0}, \tag{4b}$$

$$\sigma_x = \sqrt{\frac{\mu_{2,0}}{\mu_{0,0}} - \left(\frac{\mu_{1,0}}{\mu_{0,0}}\right)^2}, \tag{5a}$$

$$\sigma_z = \sqrt{\frac{\mu_{0,2}}{\mu_{0,0}} - \left(\frac{\mu_{0,1}}{\mu_{0,0}}\right)^2}. \tag{5b}$$

[7] Image reconstruction from moment values is a long-standing and continued area of research driven by applications to pattern recognition, image compression, and inverse theory [e.g., *Teh and Chin*, 1988; *Milanfar et al.*, 1996]. Approaches include maximum entropy reconstruction, Taylor-series approximations, and orthogonal series expansion. *Teague* [1980] demonstrated a Taylor-series moment-matching approach to reconstruct an image from its geometric moments, but the resulting images were shown to contain substantial artifacts because higher-order geometric moments contain redundant information and are highly correlated. As an alternative, Teague proposed use of orthogonal moments for compact image description and reconstruction. Whereas $x_i^p z_i^q$ terms serve as basis functions for geometric moments, various orthogonal polynomials (e.g., Legendre, Zernike, and Chebyshev) are used for orthogonal moments. Here, we use Legendre moments, λ:

$$\lambda_{p,q} = \frac{(2p+1)(2q+1)}{4} \sum_{i=1}^{nx' \cdot nz'} P_p(x_i') P_q(z_i') m_i \Delta x' \Delta z' \tag{6}$$

where x' and z' are transformed coordinates, defined on the unit square $[-1 \le x', z' \le 1]$ and $\Delta x'$ and $\Delta z'$ are the horizontal and vertical pixel dimensions for the transformed, unit-square grid. $P_m(x_i')$ is the p^{th}-order Legendre polynomial evaluated by numerical integration over cell i.

[8] As with equation (2), we recast equation (6) in matrix form, $\boldsymbol{\lambda} = \mathbf{Pm}$, where $\mathbf{P}$ includes the Legendre polynomial products for the image grid. We note that a given Legendre moment is a linear combination of geometric moments of equal and lesser order, and vice-versa, as demonstrated by *Teague* [1980]; hence we can define an invertible matrix $\mathbf{L}$ such that $\boldsymbol{\lambda} = \mathbf{L}\boldsymbol{\mu}'$, and $\boldsymbol{\mu}' = \mathbf{L}^{-1}\boldsymbol{\lambda}$, where $\boldsymbol{\mu}'$ is a vector of geometric moments also calculated on the unit square. The coordinate transformation to $[-1 \le x', z' \le 1]$ is required because Legendre polynomials are orthogonal only on the unit square. Assuming with no loss of generality that the original grid has origin (0, 0), the transformed and original geometric moments are related by

$$\mu_{p,q}' = \sum_{i=1}^{nx \cdot nz} m_i x_i'^p z_i'^q \Delta_x' \Delta_z' = \sum_{i=1}^{nx \cdot nz} \frac{x_i'^p}{x_i^p} \frac{z_i'^q}{z_i^p} \frac{\Delta x'}{\Delta x} \frac{\Delta z'}{\Delta z} \mu_{pq}, \tag{7}$$

which can be cast as the matrix operation, $\boldsymbol{\mu}' = \mathbf{B}\boldsymbol{\mu}$, where the elements of $\mathbf{B}$ contain the coordinate and discretization products in equation (7).

[9] The matrices $\mathbf{L}$ and $\mathbf{B}$ allow us to relate geometric and orthogonal Legendre moments of an image using simple matrix operations. We now take advantage of the primary use of orthogonal moments: the capability to reconstruct an image from its orthogonal moments using a truncated series expansion [*Teague*, 1980]:

$$m_i^{recon} = \frac{(2p+1)(2q+1)}{4} \sum_{p=0}^{N} \sum_{q=0}^{p} \lambda_{p-q,q} P_{p-q}(x_i') P_q(z_i') \tag{8}$$

where m_i^{recon} is the reconstructed image parameter for pixel i and N is the maximum order of moments used for the reconstruction, max(p + q).

[10] In matrix form, equation (8) is $\mathbf{m}^{recon} = \boldsymbol{\Gamma}\boldsymbol{\lambda}$, where $\boldsymbol{\Gamma}$ includes the Legendre polynomial product coefficients for the orthogonal moments. The reconstruction assumes moments of order greater than N to be zero; hence the accuracy of the image compression/reconstruction increases with the maximum order of moments considered. Description of simple images may require N < 10, whereas description of photographs may require N > 100. Together, equations (6) and (8) allow us to go between an image and its moments.

[11] To model the moment-resolving power of a tomography experiment, we use (1) the model resolution matrix

for the inversion; (2) the image reconstruction from moments; and (3) matrix manipulations to relate Legendre and geometric moments and transform between an arbitrary grid and the unit square. This yields a new moment-resolution matrix, such that $\hat{\mathbf{m}} \approx \mathbf{R}^{(\mu)}\boldsymbol{\mu}$. By combining the matrix forms of equations (1), (2), (7), and (8), with the relation between geometric and Legendre moments:

$$\mathbf{R}^{(\mu)} = \mathbf{G}\mathbf{R}\Gamma\mathbf{L}\mathbf{B} \tag{9}$$

This new resolution matrix shows that the moments calculated from a tomogram are linear combinations of the moments of the true image. For example, the vertical center of mass of the tomogram is a function of the true center of mass, spread, kurtosis, etc. Equation (9), therefore, can be used to understand reliability of, and possible bias in, the moments inferred from tomograms for given regularization criteria, survey geometries, and error models.

[12] Our derivation of $\mathbf{R}^{(\mu)}$ is only semi-analytical because it relies on an image reconstruction whose accuracy depends on the maximum order, N, of the Legendre moments considered; i.e., the derivation of equation (9) assumes equation (8) provides an adequate image reconstruction. For larger N, the $\mathbf{R}^{(\mu)}$ provides a better approximation but models the predicted moments as functions of true moments up to order N; thus there is a certain tradeoff between accuracy and ease of interpretation. High-order moments are difficult to conceptualize in terms of simple, geometric characteristics. For hypothetical targets that follow parametric probability distributions, high-order moments are simple functions of low-order moments according to the particular distribution's moment-generating equation (MGE). For example, a Gaussian-plume target is described completely by moments up to order 2. In the examples that follow, which focus on Gaussian targets, we use equation (9) and the Gaussian MGE to develop formulae for estimated plume moments in terms of true moments up to order 2. We stress, however, that adoption of the Gaussian MGE, or any MGE, is not integral to our approach, but only facilitates interpretation.

3. Examples

[13] A series of numerical examples is used to demonstrate our approach and evaluate the reliability of moment-inference from tomograms. We use both (1) linear, straight-ray difference-attenuation radar tomography and (2) non-linear, electrical resistance tomography (ERT), to image three Gaussian plumes of an electrically conductive saline tracer (Figure 1a). We use equation (10) to relate fluid conductivity, σ_f, and total dissolved solids (*TDS*); Archie's Law (equation (11)) to relate fluid and bulk electrical conductivity, σ_b; and a high-frequency approximation to relate electrical conductivity and difference attenuation, $\Delta\alpha$ (equation (12)):

$$\sigma_f = TDS/6500 \tag{10}$$

$$\sigma_b = \sigma_f \theta^{1.3}, \text{and} \tag{11}$$

$$\Delta\alpha = 1.68 \times 10^3 \Delta\sigma \frac{v}{c} \tag{12}$$

where conductivities are in units of S/m; *TDS* is in mg/l; θ is porosity, assumed to be 0.3; v is EM-wave propagation velocity, assumed to be 60×10^6 m/s; c is the speed of light in a vacuum; and $\Delta\alpha$ is in dB/m.

[14] We assume a 20-m by 20-m cross sectional domain and consider three different plume targets at different locations. The ERT grid includes additional cells on the sides and bottom of the cross section to push boundaries away from the region of interest. A least-squares Occam inversion is performed for both radar and ERT inversion. For each inversion, a line search is performed to identify the value of the trade-off parameter such that measurements are matched to a target root-mean squared error consistent with the assumed measurement errors. A series of examples is used to evaluate the accuracy of moments estimated from tomograms given changes in (1) plume location within the cross section; (2) regularization criteria, including smallness, where $\mathbf{D}$ is an identity matrix, and deviations from the background value (zero for difference tomography) are penalized; and smoothness, where $\mathbf{D}$ is a second-derivative, finite-difference operator and image roughness is penalized; (3) standard error levels; and (4) symmetric versus asymmetric survey geometries (Figure 1). The symmetric radar survey geometry consists of 1261 cross-hole measurements for raypaths between sources and receivers at 0.5-m intervals in each borehole, with a maximum vertical offset of 10 m between sources and receivers. The asymmetric radar geometry includes additional vertical-radar profile (VRP) raypaths between sources on the right side of the cross section, in 0.5-m increments, and receivers located across the land surface in 0.5-m increments. The ERT geometry consists of 1927 quadripoles, including both cross- and in-well dipoles and a surface array.

[15] The inversions produce blurry, blunted versions of reality for all targets, survey geometries, regularization criteria, and error levels considered (Figure 1). In all cases, the tomograms underpredict the magnitude of the target anomaly and overpredict its extent. Comparing results for different targets and inversions, it is evident that, in general, (1) the total mass is well resolved for radar tomography but not for ERT; (2) the vertical center of mass is somewhat resolved, (3) the lateral center of mass is poorly resolved; (4) the vertical spread is overpredicted; and (5) the horizontal spread is severely overpredicted. Although the geophysical anomalies appear visually to resolve the lateral center of mass, the blurring and streaking inherent to tomography pulls the center of mass away from the peak (the white lines in Figures 1b–1f); this is analogous to the effect of a tail on the mean of a statistical distribution, where outliers pull the mean away from the mode. Indeed, for the difference-attenuation radar examples, the lateral center of mass lies exactly at the image center for cases without VRP data. Although the additional VRP data help to resolve lateral center of mass, the asymmetric survey geometry results in highly variable resolving power, depending on the location of the plume (Figure 1d). *Milanfar et al.* [1996]. analytically showed for straight-ray tomography that estimation of image moments is impeded by limited view angles, or raypath geometry. The survey cross-hole

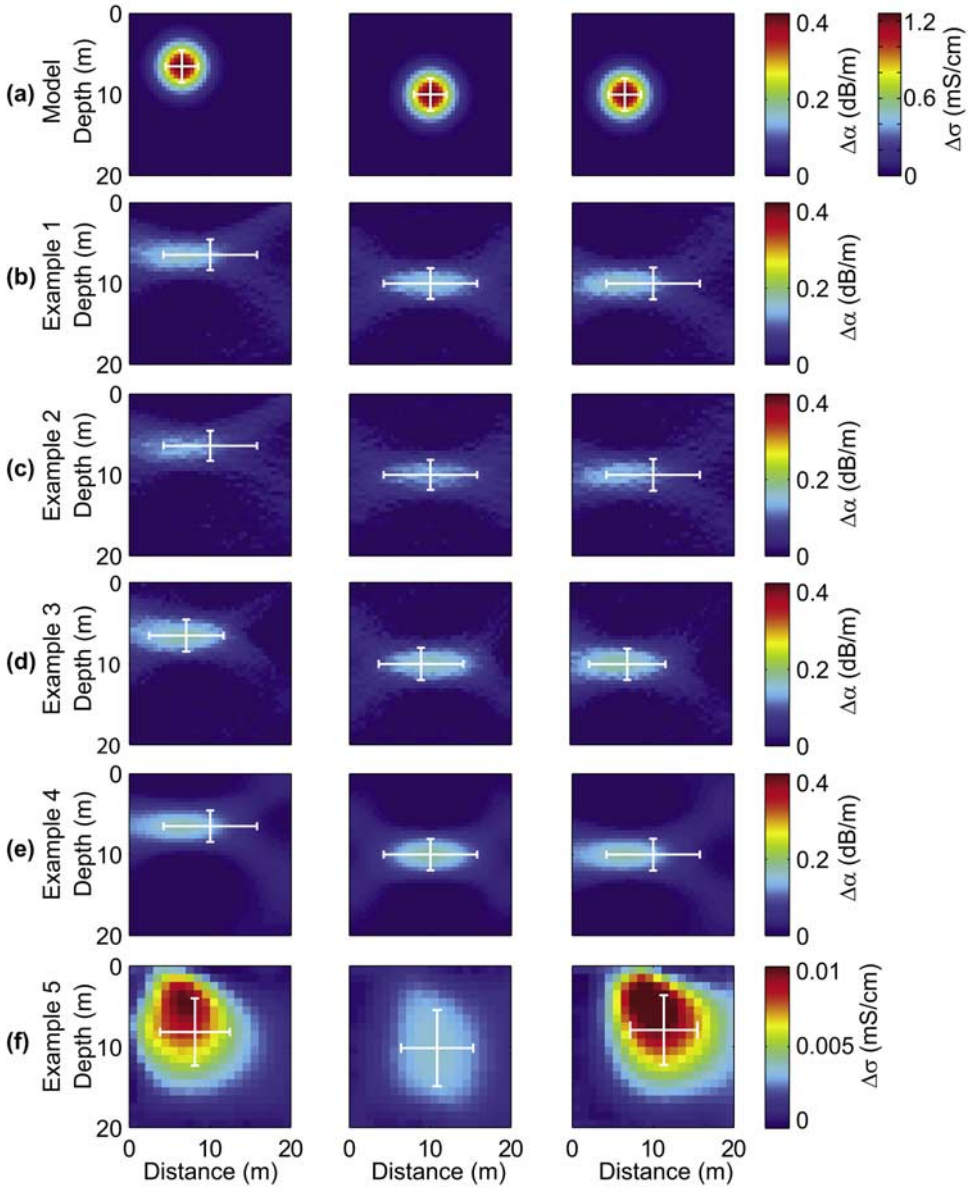

Figure 1. (a) Three synthetic models; (b) radar tomograms for 5% data error, smallness regularization, and cross-hole survey geometry; (c) radar tomograms for 10% data error, smallness regularization, and cross-hole survey geometry; (d) radar tomograms for 5% data error, smallness regularization, and asymmetric cross-hole/VRP geometry; (e) radar tomograms for 5% data error, smoothness regularization, and cross-hole survey geometry; and (f) electrical-resistivity tomograms for 5% data error and smoothness regularization. The white lines indicate the center of mass and the vertical and lateral standard deviation inferred from the tomograms.

geometry considered here is incapable of resolving the lateral center of mass. Blurring of the target also results in greater spread than in reality, with the blurring more pronounced in the lateral direction. We can use equation (9) for more rigorous quantification of these findings.

[16] We use $\mathbf{R}^{(\mu)}$ and the Gaussian MGE to derive semi-analytical expressions for the moments of the inverted image in terms of the true moments, using moments up to order 15 ($N = 15$) for the image reconstruction. Note that yet higher order moments could be used for the image reconstruction, but plumes are commonly described adequately by moments up to order 4 or 5. Figure 2 shows graphically the functions to predict the total mass, center of mass, and spatial spread for Example 1, for difference-attenuation tomography with 5% standard error and smallness-based regularization. Resolution varies spatially over the tomogram, as demonstrated and quantified by the new moment resolution matrix. To summarize, Figure 2 indicates that for radar tomography:

[17] 1. Mass recovery varies spatially and is worst for plumes centered near the lateral edges of the cross section (Figure 2a).

[18] 2. Consistent with results in Figure 1, the horizontal center of mass is completely unresolved, and is inferred to coincide with the middle of the tomogram regardless of the plume's true location (Figure 2b).

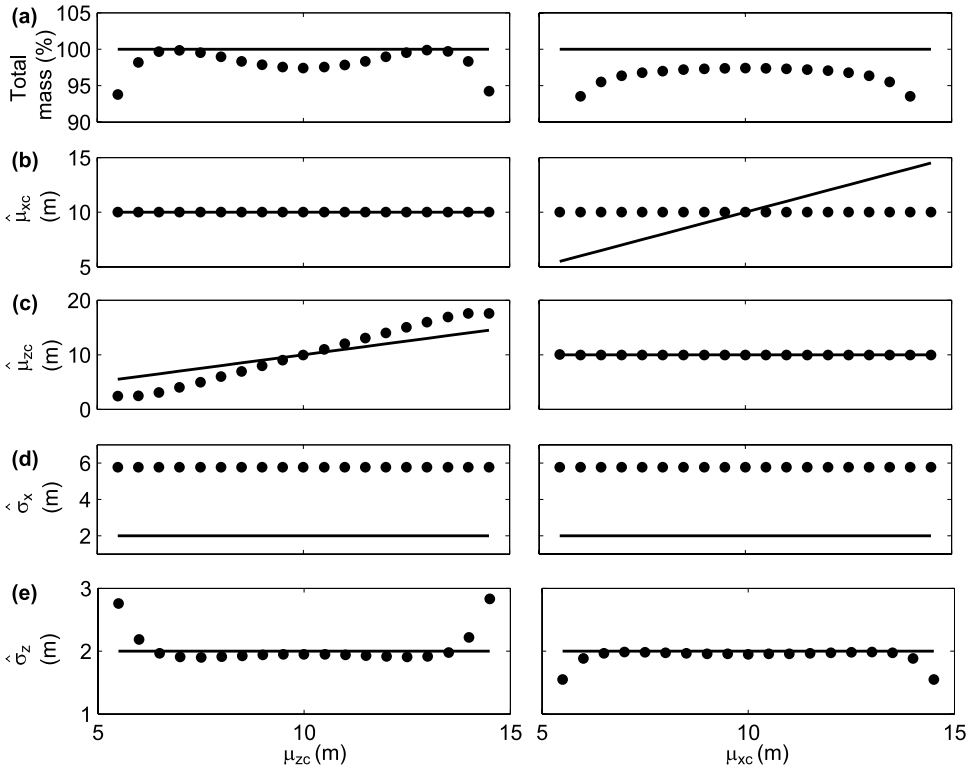

Figure 2. As functions of (left) the true vertical center of mass and (right) horizontal center of mass for Example 1: the predicted (a) total mass (b) center of mass along the x direction (μ_{xc}); (c) center of mass along the z direction (μ_{zc}); (d) spatial spread along the x direction (σ_{xc}); and (e) spatial spread along the z direction (σ_{zc}). Points indicate the predicted values calculated using the moment-resolution matrix, and lines show the true values calculated from the original image.

[19] 3. The vertical center of mass is well resolved except for cases where the plume is centered at the top- or bottom-center of the tomogram (Figure 2c).

[20] 4. The horizontal spread is poorly resolved and biased; it is overpredicted to the same extent regardless of plume location (Figure 2d).

[21] 5. The vertical spread is generally well resolved but is overpredicted for plumes centered near the vertical edges of the cross section and underpredicted for plumes near the horizontal edges (Figure 2e).

[22] These results are, of course, specific to the survey designs, measurement error, and regularization considered here. For this example, the moment values predicted using the new moment resolution matrix (i.e., $\mathbf{R}^{(\mu)}\,\boldsymbol{\mu}$) are generally within several percent of the moment values calculated using the conventional $\mathbf{R}$ and the true model parameters (i.e., $\mathbf{GRm}$). We note that the semi-analytical approach tends to provide a superior match to the true moments than direct calculation on synthetic tomograms, which can be affected by individual random error if errors are large relative to the measurements. Our results, therefore, should be considered as "best-case" scenarios for assessment of field-experimental designs.

4. Discussion and Conclusions

[23] Geophysical tomography provides valuable qualitative insight into the morphology of plumes associated with tracer tests, natural processes, and engineered remediation. Increasingly, tomograms are used for inference of plume moments, in efforts to gain quantitative insight into underlying transport processes (i.e., advection, dispersion, and rate-limited mass transfer). We derived a semi-analytical moment-resolution matrix to relate the moments of an inverted tomogram to the moments of the underlying, true image. Our derivation is based on (1) the classic model resolution matrix, and (2) an orthogonal series-expansion approach for image reconstruction from moment values. The accuracy of the latter depends on the maximum order of moments considered, whereas the accuracy of the former depends on the linearity of the inversion and the reliability of the prior model of measurement error. The new moment resolution matrix provides a framework to quantify the effects of survey geometry, measurement error, regularization criteria, and plume location on estimated moment values.

[24] A series of numerical examples demonstrated the utility of our new moment resolution matrix. For the straight-ray radar and electrical-resistivity tomography examples considered, our results indicate that moment inference from tomograms is prone to considerable bias: the total mass of target plumes was underestimated, the spatial spread was overestimated, and the lateral center of mass was resolved poorly or not at all. These findings vary depending on survey geometry, mode of tomography (e.g., electrical resistivity versus radar), parameterization, and inversion approach (i.e., non-linear versus linearized inversion); nonetheless, our results clearly demonstrate that (1) in

many practical applications, moments inferred from tomograms are subject to substantial bias and error, and may result in misleading interpretations of plume morphology and underlying transport behavior; and (2) the new moment resolution matrix is a useful tool to understand and quantify the limitations of moment inference from tomograms.

[25] **Acknowledgments.** This work was supported by the U.S. Geological Survey Toxic Substances Hydrology Program, the National Science Foundation through grant 0440322, and the American Chemical Society through PRF grant 45206-G8. The authors are grateful to Lee Slater (Rutgers University), Adam Pidlisecky (Stanford University) and John W. Lane Jr. (USGS) for technical reviews of the manuscript.

References

Binley, A., G. Cassiani, R. Middleton, and P. Winship (2002), Vadose zone flow model parameterisation using cross-borehole radar and resistivity imaging, *J. Hydrol.*, *267*, 147–159.

Day-Lewis, F. D., and J. W. Lane Jr. (2004), Assessing the resolution-dependent utility of tomograms for geostatistics, *Geophys. Res. Lett.*, *31*, L07503, doi:10.1029/2004GL019617.

Day-Lewis, F. D., J. W. Lane Jr., J. M. Harris, and S. M. Gorelick (2003), Time-lapse imaging of saline-tracer transport in fractured rock using difference-attenuation radar tomography, *Water Resour. Res.*, *39*(10), 1290, doi:10.1029/2002WR001722.

Day-Lewis, F. D., K. Singha, and A. M. Binley (2005), Applying petrophysical models to radar travel time and electrical resistivity tomograms: Resolution-dependent limitations, *J. Geophys. Res.*, *110*, B08206, doi:10.1029/2004JB003569.

Harvey, C. F., and S. M. Gorelick (1995), Temporal moment-generating equations: Modeling transport and mass transfer in heterogeneous aquifers, *Water Resour. Res.*, *31*(8), 1895–1911.

Hubbard, S. S., J. Chen, J. Peterson, E. L. Majer, K. H. Williams, D. J. Swift, B. Mailloux, and Y. Rubin (2001), Hydrogeological characterization of the South Oyster Bacterial Transport Site using geophysical data, *Water Resour. Res.*, *37*(10), 2431–2456.

Lane, J. W., Jr., F. D. Day-Lewis, R. J. Versteeg, and C. C. Casey (2004), Object-based inversion of cross-well radar tomography to monitor injection experiments, *J. Environ. Eng. Geophys.*, *9*(2), 63–77.

Lane, J. W., Jr., F. D. Day-Lewis, and C. C. Casey (2006), Geophysical monitoring of field-scale vegetable oil injections for biostimulation, *Ground Water*, *44*(3), 430–443, doi:10.1111/j.1745-6584.2005.00134.x.

Milanfar, P., W. C. Karl, and A. S. Willsky (1996), A moment-based variational approach to tomographic reconstruction, *IEEE Trans. Image Process.*, *5*(3), 459–470.

Singha, K., and S. M. Gorelick (2005), Saline tracer visualized with three-dimensional electrical resistivity tomography: Field-scale spatial moment analysis, *Water Resour. Res.*, *41*, W05023, doi:10.1029/2004WR003460.

Singha, K., and S. M. Gorelick (2006), Effects of spatially variable resolution on field-scale estimates of tracer concentration from electrical inversions using Archie's law, *Geophysics*, *71*(3), G83–G91.

Teague, M. R. (1980), Image analysis via the general theory of moments, *J. Opt. Soc. Am.*, *70*(8), 920–930.

Teh, C., and R. T. Chin (1988), On image analysis by the method of moments, *IEEE Trans. Pattern Anal. Mach. Intell.*, *10*(4), 498–513.

Y. Chen, Center for Integrative Geosciences, University of Connecticut, 238 Beach Hall, Storrs, CT 06268, USA. (yoc03001@engr.uconn.edu)

F. D. Day-Lewis, U.S. Geological Survey, Office of Ground Water, Branch of Geophysics, 11 Sherman Place, Unit 5015, Storrs, CT 06269, USA. (daylewis@usgs.gov)

K. Singha, Department of Geosciences, Pennsylvania State University, 311 Deike Building, University Park, PA 16802, USA. (ksingha@psu.edu)